Journal of Hazardous Materials xxx (xxxx) xxx

Contents lists available at ScienceDirect

Journal of Hazardous Materials

journal homepage: www.elsevier.com/locate/jhazmat

Identification and characterisation of individual nanoplastics by scanning transmission X-ray microscopy (STXM)

Alexandra Foetisch [a], Montserrat Filella [b], Benjamin Watts [c], Laure-Hélène Vinot [a], Moritz Bigalke [a,*]

[a] Institute of Geography, University of Bern, Hallerstrasse 12, 3012 Bern, Switzerland
[b] Department F.-A. Forel, University of Geneva, Boulevard Carl-Vogt 66, CH-1205 Geneva, Switzerland
[c] Paul Scherrer Institute, Forschungsstrasse 111, 5232 Villigen, Switzerland

ARTICLE INFO

Editor: Dr. T. Meiping

Keywords:
Nanoplastic analysis
Soil pollution
Environmental pollution
Scanning transmission X-ray microscopy

ABSTRACT

Nanoplastics (NP) are of environmental and human health concern. We tested a novel NP extraction method and scanning transmission X-ray spectro-microscopy (STXM) in combination with near-edge X-ray absorption fine-structure spectroscopy (NEXAFS) to image and identify individual NP in environmental and food matrices. We (1) discussed the potential of STXM compared to other methods potentially suitable for NP analysis, (2) applied the method on NP suspensions of eight of the most common polymers, (3) analyzed environmental water and soil samples spiked with NP and (4) characterized NP in tea water infused in plastic teabags and unspiked soil samples. Here we show that STXM has methodological advantages and that polymers give characteristic spectra, which allows NP identification in environmental and food matrices. For soils we deliver a visual and spectroscopic characterization of NP, proving their presence and highlighting their diversity. Thus, STXM, can be used for the detection and characterisation of NP in different types of matrices.

1. Introduction

Since 1950, about 8300 million metric tons of plastic have been produced worldwide, 79% of which are accumulated in landfills or in the environment (Geyer et al., 2017). Among the diversity of plastic waste generated, nanoplastics (NP), plastics of a size < 1 μm, are of environmental importance. They can be either released directly from manufactured products or produced by the physical, chemical or mechanical degradation of larger polymer objects. As several studies on microplastics (MP) have shown that the particle size distribution found in the environment is heavily skewed towards the smallest detectable particles (Enders et al., 2015; Fok et al., 2017; Scheurer and Bigalke, 2018), one can expect NP to be present in high numbers. However, research on NP occurrence in the environment is in its infancy and limited monitoring data are available (Jiang et al., 2020). Indeed, infrared (IR) and Raman spectroscopy as commonly used in MP research have a resolution limited to the > 10 μm and > 1 μm size range, respectively (Schwaferts et al., 2019). Chromatographic analysis of pyrolysis products or extracted polymers allow for the identification of polymers but do not provide any information on the size or shape of the particles analysed (Ter Halle et al., 2017; Duemichen et al., 2019). Yet, all these characteristics are critical to assess any potential NP environmental effect. Until now, the behavior and fate of NP in the environment have mostly been studied using artificial NP labeled with metals, fluorescent dyes or enriched stable isotopes (Mitrano et al., 2019; Sander et al., 2019; Li et al., 2020).

Here, we demonstrate how scanning transmission X-ray spectro-microscopy (STXM) can be effectively applied for imaging and identifying NP in different environmental matrices. For this purpose, we (1) discuss analytical techniques potentially suitable for NP analysis and introduce STXM, (2) purchased or produced NP of polypropylene (PP), polyethylene (PE), polyvinyl chloride (PVC), polyethylene terephthalate (PET), polystyrene (PS), polyamide (PA), polycarbonate (PC) and polymethylmetacrylate (PMMA) and acquired STXM images and NEXAFS spectra of individual NP to confirm the suitability of this technique to identify and characterize plastics in the nano size range, (3) developed an extraction protocol, combined it with STXM and tested it for NP extraction from spiked water and soil samples and (4) analyzed unspiked samples like tea from plastic tea bags and natural soil samples to test the application of the method on environmental and food matrices.

* Corresponding author.
E-mail address: moritz.bigalke@giub.unibe.ch (M. Bigalke).

https://doi.org/10.1016/j.jhazmat.2021.127804
Received 6 August 2021; Received in revised form 8 November 2021; Accepted 11 November 2021
Available online 16 November 2021

2. Methods

2.1. Nanoplastic materials

We purchased or produced nanoparticles suspension of eight common polymers. Pellets of PA Radilon, PC Makrolon, LDPE Lupolen, HDPE Hostalen, PMMA Altuglas, PP Moplen and PVC lab bottles were provided by Semadeni Plastics group, Switzerland. NP preparation was performed by adapting previously published methods (Astner et al., 2019). In a first cryogrinding step, 60 – 80 g of the initial material was grinded twice for 10 s with a Pulverisette 11 (Fritsch, Germany) in liquid nitrogen. The resulting powder was then sieved and the fractions < 250 μm or < 63 μm (depending on the available mass) were collected and milled in a cryogrinding jar with 15 mm or 3 mm stainless steel beads. The jar was sealed, frozen into liquid nitrogen and shaken at a frequency of 28 Hz for 5 min with a mixer mill (MM 400, Retsch GmbH, Haan, Germany). The freezing and grinding steps were repeated ca. 40 times to maintain the brittleness of the material while grinding. A portion of the resulting powder was suspended in 600 μL ethanol (≥ 99.8%, Prod.-No 51976, Sigma Aldrich, USA) and allowed to settle for 5 min before collecting the nanoparticle-containing supernatant. Protocols specific to each polymer are available in the supplementary material (Table S1). Nanoparticles of PET were produced from a regular transparent PET water bottle (M-Budget still water, Switzerland) by adapting an existing method (Rodríguez-Hernández et al., 2019). Fluorescent PS nanobeads of 100 nm (micromer®-redF, plain, 30–00–102) and 250 nm (micromer®-greenF, plain, 29–00–252) were purchased from Micromod, Germany. White, non-fluorescent 500 nm PS beads (95585–5 mL-F) were purchased from Sigma-Aldrich (USA).

2.2. Natural water and soil samples

A water sample was collected in Lake Luzern (47°02'31.5"N 8°19'52.9"E, Switzerland) in November 2020 with a 3 m pole and a glass bottle from a pontoon at the outflow of the lake. The water sample had a conductivity of 210 μS cm^{-1} and was kept refrigerated until spiking it with a mix of approximately 0.07 g PC, 0.3 g PMMA and 3 g PP powders resulting from the cryogrinding and 10 mL of suspended PET particles to 1 L of the lake water sample. Soil samples were collected in the mountains in Laax (GR, Switzerland) at a site which did not contain any MP (Scheurer and Bigalke, 2018). This clean soil was spiked with approximately 1 g of PA powder or 41 μL of 250 nm PS beads in 50 g of soil to test the extraction analysis. Further soil was sampled at two agricultural fields in Sant'Antonino (SAN; TI, Switzerland) and Gampelen (GAM; BE, Switzerland) with a history of mulch foil application and irrigation and two roadside soils in Belpberg Dufti (DUF; BE, Switzerland; 8 m wide rural street, 2 m from the road) and Wohlen bei Bern, Breitacher (BRA; BE, Switzerland; 6 m wide rural street, 10 m from the road), respectively. These soils were not spiked but analyzed to observe the NP composition of their respective localities. Green and peppermint tea in plastic teabags were purchased from a local grocery store.

2.2.1. Water and soil samples extraction

All equipment used for the extraction of NP was cleaned first with a brush, soap and water, ultrasonicated for 10 min, rinsed with ethanol, rinsed with MilliQ water and finally dried under a laminar flow clean bench (FMS SuSi, Spetec, Erding, Germany). All work except the ultracentrifugation was done on the clean bench with HEPA (H14) filtered air and all-cotton lab coats were worn.

Soil samples (50 g) were suspended in 1 L of 2.5 mM ultrafiltrated (<10 kDa, Amicon Stirred Cell, Merck Millipore, Sigma Aldrich, USA) tetrasodium pyrophosphate (TSPP, $Na_4P_2O_7$, > 95%, Sigma Aldrich, USA), shaken for 30 min at 100 rpm, ultrasonicated for 2 min with a Labsonic L (B. Braun, Switzerland) at a frequency of 20 kHz and a power of 100 W, and then allowed to settle for 18 h (Schwertfeger et al., 2017). Then, 30 mL of solution were collected from the surface with a glass volumetric pipette and transferred into a new glass vial. A 5 mL aliquot of sucrose solution (≥ 99%, Sigma Aldrich, USA) of a density 1.37 g mL^{-1} (1220 g L^{-1} MilliQ water) was deposited at the bottom of 38.5 mL polyclear tubes (25–30–70, Hemotec, Switzerland) while carefully avoiding to deposit any drops on the tube wall. 30 mL of the solution collected after settlement was then gently deposited on the top of the sucrose solution and the tubes were centrifuged at 22,000 rpm (acceleration of approx. 109.500 *g*) for 2 h (Ultracentrifuge CP100NX, HITACHI, Japan) for the mineral particles (density >1.37 g mL^{-1}) to migrate through the sucrose to the bottom of the centrifuge tube. After centrifugation, the upper solution and the upper 5 cm (~2 mL) of the sucrose were collected with a pipette and transferred to a new glass vial. Then, the walls of the tubes were rinsed with ethanol, which was also collected with a pipette and added to the first supernatant. In order to oxidize the remaining natural organic matter (NOM) and sucrose from solution, hydrogen peroxide (H_2O_2, 30%, Sigma Aldrich, USA) solution was added to the samples to reach a concentration of a 5% (v/v). The addition was repeated every 2 h for 22 h. This treatment was chosen to avoid high H_2O_2 concentrations in the samples which could oxidize NP. The dissolved C in the sample was analyzed with a DOC analyzer (DIMATOC 2000, Dimatec, Essen, Germany), by combustion of the sample and detection of the released CO_2. After every 2 h the 5% H_2O_2 are consumed by the oxidation of the sucrose and OM in the sample, so that the H_2O_2 concentration never exceeds 5% (Fig. S1a). After about 11 additions, the concentration of dissolved C in the sample showed only a slow decrease, so that no further H_2O_2 was added (Fig. S1b). After this treatment, samples were washed and concentrated using an ultrafiltration cell (Amicon Stirred Cell, Merck Millipore, Sigma Aldrich, USA) with a < 10 kDa polyethersulfone membrane (Biomax Ultrafiltration Discs, Sigma Aldrich, USA). The samples were transferred into the ultrafiltration cell and the cell volume was completed (200 mL) with MilliQ water. The sample was then filtrated until approx. 10 mL of solution remained. The last two steps were repeated three times to further wash dissolved compounds (TSPP, sucrose, salts, etc.) from the sample. The 10 mL of sample remaining in the cell at the end of the procedure was transferred into a clean glass vial and the ultrafiltration membrane was rinsed with 10 mL of ethanol (≥ 99.8%, Prod.-No 51976, Sigma Aldrich, USA). Our final soil extract was thus a suspension in a 50:50 ethanol:water solution.

2.2.2. Spiked water and soil samples extraction

NP in tea were produced following the procedure described in a previous study (Hernandez et al., 2019) except that in our experiment the tea was kept in the tea bag during preparation to have a realistic matrix for the analysis of food samples. A single tea bag of each tea was soaked in 12 mL 95 °C MiliQ water for 5 min. The spiked water and the tea samples were treated with the same procedure than the soil samples except without the first extraction step with the TSPP, which was not necessary for liquid samples. Thus spiked water and tea samples were treated with a density separation step, an oxidation of organic matter step, a washing step in the ultrafiltration cell and finally deposited on the membrane for analysis.

2.3. STXM sample preparation

Standard (SiRN-5.0–200–1.0–100) and finder (with gold finder grid; SiRN-5.0–200–1.0–100+G1Au20) membranes (1 × 1 mm, 100 nm thick Si_3N_4 windows) were purchased from Silson (UK) Nanoplastic particles were placed on the membranes either by drop deposition (particles from pure plastic suspensions; the membrane was tilted to reduce the coffee ring effect) or by sedimenting the particles out of the 50:50 water: ethanol solution onto the membrane fixed to the bottom (via an aluminium holder) of a 15 mL glass centrifuge tube for 3.5 h at 3400 *g* (for particles which where extracted from soil, tea and water samples). Some membranes with finder grid were analyzed by SEM (Gemini 450, Zeiss; JSM7001F, JEOL) prior to or after STXM measurements with the

aim of either localising particles more quickly on the membrane during the STXM measurement or of acquiring a high-resolution picture of NP. A voltage of 15 and 10 kV was used with secondary-electron in-lens detector and membranes were coated with a c.a. 5 nm gold layer. After recognizing the serious radiation damage caused by SEM analysis prior to STXM (Fig. S2), samples were only imaged by SEM after the STXM analysis.

2.4. Data acquisition and processing

The STXM measurements were performed at the PolLux beamline of the Swiss Light Source (SLS) synchrotron at the Paul Scherrer Institute in Villigen, Switzerland. The detailed beamline layout has been described before (Raabe et al., 2008). A 25 nm zone plate was used to focus the monochromated soft X-ray beam (spot size of ~30 nm) on the membrane and particles were imaged by raster scanning an area of the membrane at 350 eV. Once a particle was found, a zoomed-in and focused picture was taken. NEXAFS spectra were then acquired by line or stack measurement in the energy range between 280 and 350 eV corresponding to the C K-edge. We analyzed a variety of sizes of NP for each polymer to test for which size range STXM is suitable. The acquired NEXAFS spectra were extracted with aXis2000 (http://unicorn.mcmaster.ca/aXis2000.html) and normalized and plotted with RStudio (RStudio Team, 2020) to allow comparison of the characteristic peaks for the individual NP with published reference spectra (Dhez et al., 2003). As no reference could be found for PVC, we measured our own reference on a microtomed sample. Particle size was measured on SEM and/or STXM pictures using ImageJ. The given size on this study corresponds to the longest distance between any two points along the selection boundary (Merkus, 2009; Fig. S3). The thickness is estimated by multiplying the optical density value at 320 eV by the attenuation length. The attenuation length depends mostly on the material chemical structure and density (Table S2).

3. Results and discussion

3.1. Relating STXM to other analytical methods for NP analysis

Identifying NP in environmental matrices requires the ability to interrogate individual nanoparticles, coupled with a spectroscopic tool with natural contrast (i.e. is not reliant on labeling) that is capable of providing information about molecular structure such that polymers can be distinguished from the natural organic matter that is abundant in all ecosystems. The examination of individual particles typically requires nanoscale focusing, both to isolate the signal of a single particle and to obtain sufficient signal strength. For many analytical probes, this is restricted by the Abbe diffraction limit (Abbe, 1873), which says that the probe beam cannot be focused to less than about half of its wavelength. While there exist many super-resolution strategies to circumvent this limit, they each introduce their own restrictions that may preclude their application to label-free spectroscopy. For example, super-resolution techniques based on sub-pixel localisation or the manipulation of sample fluorescence are generally unhelpful for spectroscopic applications (Wöll and Flors, 2017; Chapman et al., 2020). Further, super-resolution techniques based on near-field effects can have severely limited application to nanoparticles larger than the evanescent wave, thus excluding the majority of the nano-scale size range.

The list of analytical techniques capable of differentiating organic materials is limited by the specific need to probe the molecular structure, which is what defines the identity of an organic substance (Favre and Powell, 2014). Other physical properties such as the density, or constituent elements of an organic substance are not indicative of the molecular structure and therefore do not make a significant contribution toward material identification. Vibrational spectroscopies, such as IR and Raman spectroscopy indicate the characteristic oscillations of functional groups within the sample, and so provide an excellent probe for differentiating organic materials (Hashimoto et al., 2019). While the visible wavelengths used for Raman allow sub-micron focusing and optical trapping of nanoparticles (Penders et al., 2018; Gillibert et al., 2019), the signal is typically very weak and easily overwhelmed by fluorescence effects. Recently, Raman spectroscopy was coupled with scanning electron microscopy (Zhang et al., 2020) to spectroscopically identify sub-micron particles and PVC NP. While technically fulfilling the requirements for nanoscale imaging and spectroscopy, this characterization strategy may not be generally applicable to all NP characterizations. Firstly, the Raman signal to noise ratio is expected to deteriorate rapidly as the particle size decreases below the spatial resolution of the visible laser probe. Secondly, it is our experience that some polymer types are very sensitive to electron beams (Fig. S1) such that particle spectra are modified beyond recognition after SEM imaging. Applications of IR spectroscopy to nanoparticles require a super-resolution technique (Nan et al., 2020). Nuclear magnetic resonance (NMR) can be used to identify molecular structures and, although super-resolution techniques are routinely applied to exceed the Abbe diffraction limit of the radio-frequency excitation pulses, sub-micron resolution is difficult to attain (Glover and Mansfield, 2002). However, nanoscale NMR measurement has been demonstrated by exploiting the extreme sensitivity of near-surface nitrogen-vacancy defects in diamond (Mamin et al., 2013). Mass spectrometry techniques such as secondary ion mass spectrometry (SIMS) measure the mass of molecular fragments blasted from the sample, the distribution of which indicate the elements and molecular groups comprising the sample material (Wien, 1997). While these probes can be focused to nanoscale resolution, the limited volume of individual nanoparticles severely restricts the statistical significance of measurements on small nanoparticles (Liang et al., 2015) unless a post-ionisation scheme is used to enhance the secondary ion yield (Popczun et al., 2017). Pyrolysis gas chromatography mass spectrometry is analogous to SIMS and while a nano-focused heat source could be implemented, the material volume provided by an individual nanoparticle is unlikely to produce convincing program statistics. The method can be applied to samples which are prior fractionated to a defined size by filtration or other separation techniques (Ter Halle et al., 2017; Wahl et al., 2021), and thus confirm the association of polymers with particles in the nano-size range. However, it cannot measure the characteristics (size, shape, molecular structure) of the individual NP. Wahl et al. (2021) used asymmetric flow-field flow fractionation to separate nanoparticles from plastic-contaminated soil extract and identified molecular species indicative of common polymers via pyrolysis gas chromatography mass spectrometry. While this method establishes the presence of nanoparticles in the soil and their association with polymer materials (or their breakdown products), it lacks evidence that any individual nanoparticles are chiefly composed of polymer. For example, inorganic nanoparticles associated or coated with polymer are also consistent with the observations by Wahl et al. (2021) but are not consistent with the common understanding that NP should consist of the same material throughout its thickness.

Finally, spectroscopies involving electronic excitations of the core shell of carbon atoms can identify the bonding schemes present in an organic material and are routinely probed by beams of electrons (electron energy loss spectroscopy; EELS) or soft X-rays (near-edge X-ray absorption fine-structure spectroscopy; NEXAFS) with nanoscale resolution (Hitchcock et al., 2008). Scanning and transmission electron microscopy (SEM/TEM) can provide excellent spatial resolution for EELS, but causes a high rate of radiation damage in organic samples (Hitchcock et al., 2008). While this radiation damage tends to not significantly alter the size and shape of the organic nanoparticles, the molecular structure, and hence the absorption spectrum, is significantly altered (Fig. S2). Note that energy dispersive X-ray spectroscopy (EDX), which is commonly performed in electron microscopes, only provides elemental composition and is unable to discern polymers from natural organic matter commonly found in the environment (Egerton, 2009).

NEXAFS spectroscopy has been successful in positively identifying polymer materials (Dhez et al., 2003; Watts et al., 2011) by measuring spectra at the carbon K-edge (near 300 eV, or about 4 nm wavelength) (Ade and Hitchcock, 2008; Watts and Ade, 2012). Soft X-rays in this spectral range can also be focused by a Fresnel zone plate for the nanoscale imaging of structures composed of polymer, biological and other organic materials (Raabe et al., 2008). Soft X-ray microscopy can be implemented in full-field, scanning and ptychographic designs, however, STXM has strong advantages for performing nano-spectroscopy of organic materials due to the ease of keeping focus while acquiring spectra and excellent radiation dose efficiency (Jacobsen, 2019). As a non-destructive technique, STXM can also be combined with complementary techniques for further analysis of NP. Thus, e.g. SEM images can be acquired after the sample analysis by STXM to observe the particles with high spatial resolution (Fig. S3) or EDX can be used to investigate metal additives within NP. To find back the particles analysed by STXM with other techniques finder membranes with a 100 × 100 µm gold grid can be used.

STXM raster-scans a sample region across a nano-focused X-ray beam to form X-ray transmission images with spatial resolution down to 7 nm (Raabe et al., 2008) (Fig. 1, a). Varying the photon energy of the incident X-ray beam allows STXM to perform X-ray spectroscopy on nanoscale objects and to use spectroscopic effects to generate quantitative contrast mechanisms based on physical and chemical properties such as elemental composition, oxidation state, molecular structure, molecular orientation and local magnetization (Ade and Stoll, 2009). The minimal optical design of STXM maximizes the radiation dose-efficiency and positioning precision, both laterally (for high spatial resolution) and along the optical axis for easy focusing, which is important for performing spectroscopy with the dispersive Fresnel zone plates required for soft X-ray nano-focusing. As a synchrotron-based method, STXM is not easily available for routine measurement in one's own lab, but can be accessed (free of charge for academic use) by any researcher after a successful application to one of the many facilities worldwide (e.g. CA, CH, CN, DE, FR, GB, JP, UK, US) (https://lightsources.org; https://wayforlight.eu).

NEXAFS spectroscopy at the carbon K-edge (X-ray photon energy near 300 eV) involves resonance peaks that correspond to photo-excited transitions from the C 1 s orbital to unoccupied molecular orbitals corresponding to anti-bonding states. The peaks will thus indicate the presence and the proportion of particular bonding types, characterising the molecular structure surrounding the absorbing C atoms. This means that C K-edge NEXAFS spectra can function as highly specific fingerprints of organic materials and there is no need for labeling or staining in order to positively identify a material. The influence of other factors such as physical state and intermolecular interactions are very small and a C K-edge NEXAFS spectrum is typically well represented simply by the sum of the spectra of its component structures (Stöhr, 1992). Moreover, in the case of C-based polymers, a given set of bonds is usually repeated many times and, thus, the corresponding C K-edge NEXAFS spectra tend to consist of strong, clearly defined resonance peaks that make them straightforward to identify (Dhez et al., 2003) (Figs. 2 a-h and S4). On the contrary, natural organic matter is normally a mixture of a broad variety of bonding types and gives nonspecific spectra (Fig. 2, i-j).

In practice, a spectro-microscopy analysis of nanoparticles deposited onto an X-ray transparent substrate can be performed in a number of ways. First, organic particles can be separated from any mineral and salt particles remaining from the sample preparation by comparing images measured with photon energies below (280 eV) and above (350 eV) the C K-edge. Materials with a high carbon content will show a strong difference in X-ray absorption between these two energies, while other materials will show little contrast. Once located, the spectrum of a particle is measured by recording the X-ray transmission through the particle location while scanning the photon energy across the C K-edge.

3.2. Nanoplastic identification

The spectra of nanoparticles composed of eight common polymers were matched with reference spectra (Dhez et al., 2003). STXM, as a transmission technique, is mostly limited by the thickness (Z dimension) of a particle and not by its size appearance in a 2D image (X and Y dimension). Particles were observed and identified down to a particle thickness of about 100 nm (Fig. 2), at which point the statistical efficiency of the technique is rapidly decreasing (Fig. S5). Note that the STXM measurements were performed on a bend-magnet beamline and that an undulator-based instrument would provide about 100 times

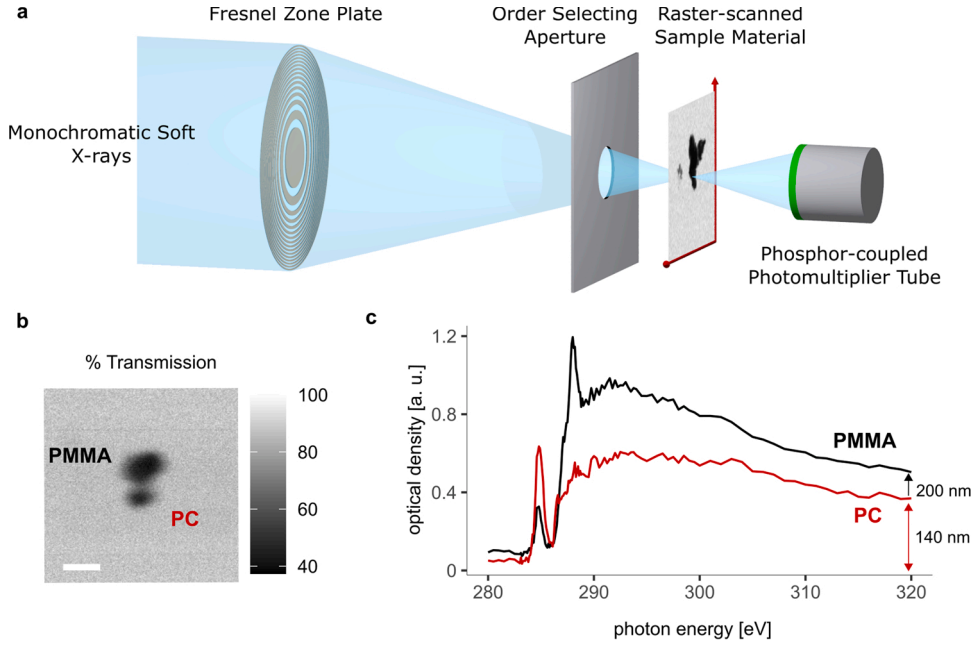

Fig. 1. Illustration of STXM principle and NEXAFS acquisition for PMMA and PC polymers. (a) Schematic illustration of the setup of a STXM instrument, (b) STXM image taken at 350 eV photon energy of a pair of particles. The white scale bar is 500 nm. (c) NEXAFS spectra of the particles in (b) and identified as PMMA and PC. The particles thicknesses are estimates from the post-edge absorbance to be 200 nm and 140 nm respectively.

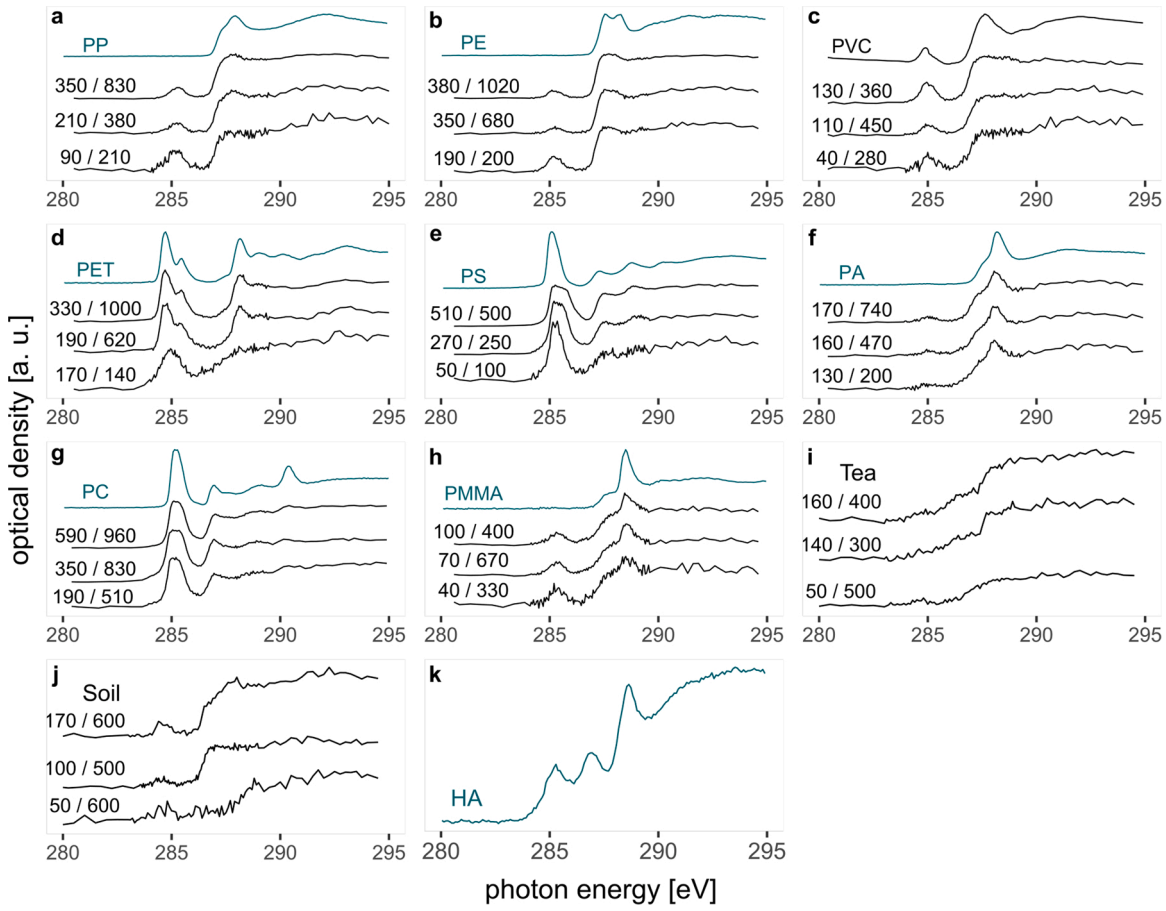

Fig. 2. Differentiation of polymers by C K-edge NEXAFS spectroscopy. (a-h) Comparison of NP spectra from eight polymers (black spectra) compared with a reference spectrum (blue) (Dhez et al., 2003). All spectra have been normalized to fit the scale. The energy position was corrected for the first peak of PS to match the reference: (a) PP, (b) PE, (c) PVC, (d) PET, (e) PS, (f) PA, (g) PC, (h) PMMA. The thickness [nm] / Feret diameter [nm] of the particle corresponding to the spectrum is written on the left hand-side of each NEXAFS spectrum. As no PVC reference spectrum was available in the literature, we measured the NEXAFS spectrum of a microtomed PVC sample. (i-j) NEXAFS spectra of common natural organic matter occurring in tea and soil, respectively. (k) Humic acid (pH =6) reference spectrum (Christl and Kretzschmar, 2007).

more X-ray flux and hence a commensurate improvement in either spectral quality or acquisition rate. In some cases, we used self-produced NP, with varying lower size limits. In line with the theoretical considerations, we observed that the spectral quality remained unchanged with respect to the lateral size of the particle but decreased with decreasing thickness of the particle, causing noisy spectra at particle thicknesses < 100 nm e.g. for the thinnest particles of PP, PVC, PS and PMMA (Fig. 2, a, c, e, h). Depending on polymer properties, mechanical grinding and chemical precipitation can lead to nanoparticles with varying shapes. The thinner a particle is, the more photons will be required to obtain a spectrum of the same quality. As particles tend to deposit with a preference to lay flat against the substrate, the shortest dimension of a particle is the one limiting its analysis.

The spectra can be attributed to specific polymers by comparing the exact position and relative intensity of the main peaks to those of reference spectra of polymers or of molecules with shared bonding structures (Dhez et al., 2003). Some of the polymers studied showed differences in the spectra compared to the references, the most common being a decrease of the main peak intensity, often accompanied by the appearance of a new peak at 285 eV (Fig. 2). These differences between experimental (Fig. 2, a-h black lines) and reference, (Fig. 2, a-h blue lines) spectra indicate radiation damage induced by the X-ray beam during the STXM analysis. Similar differences between the nanoparticle measurements and reference materials can be observed in Fig. 3. The estimated radiation dose (Table S3, Fig. S6) in many cases are above the critical doses for the alteration of carbonyl, phenyl and C-H groups in polymers, which are quite sensitive to ionizing radiation and have been systematically studied (Coffey et al., 2002; Wang et al., 2009). The most significant radiation damage effect observed in common polymers is a decrease in the C1s $\rightarrow \pi^*_{C=O}$ resonance near 287 eV, often accompanied by an increase in the C1s $\rightarrow \pi^*_{C-C}$ resonance near 285 eV, that is caused by the reduction of carbonyl groups (which produces vinyl C=C bonds). Such radiation damage is clearly seen in the spectra in Figs. 2 and 3, especially for PA and PMMA for which carbonyls dominate the molecular structure, but also for PET and PC (note that the C1s $\rightarrow \pi^*_{C=O}$ resonance for PC is shifted to 291 eV), which also contain carbonyl groups. The radiation dose could be further reduced by careful attention to the spatial scanning parameters in order to evenly spread the dose across the entirety of the limited nanoparticle volume, and by limiting the spectral quality (in terms of energy points measured and counting time) to the minimum required for identification. While the deposition of a carbonaceous layer is a common issue during STXM analysis, it appears unlikely in this case as none of our spectra show an increase at 288.5 and 293 eV, which would be typical for a carbon layer deposition (Leontowich and Hitchcock, 2012).

3.2.1. *Finding NP in spiked environmental matrices*

In environmental samples, a wide variety of particles exist simultaneously in the media and can interfere with the identification and characterisation of NP, making it difficult to find NPs simply by being present in much higher numbers. A method to extract NP from soil and water samples (Fig. 3, a; Fig. 4, a) was developed, based on methods for

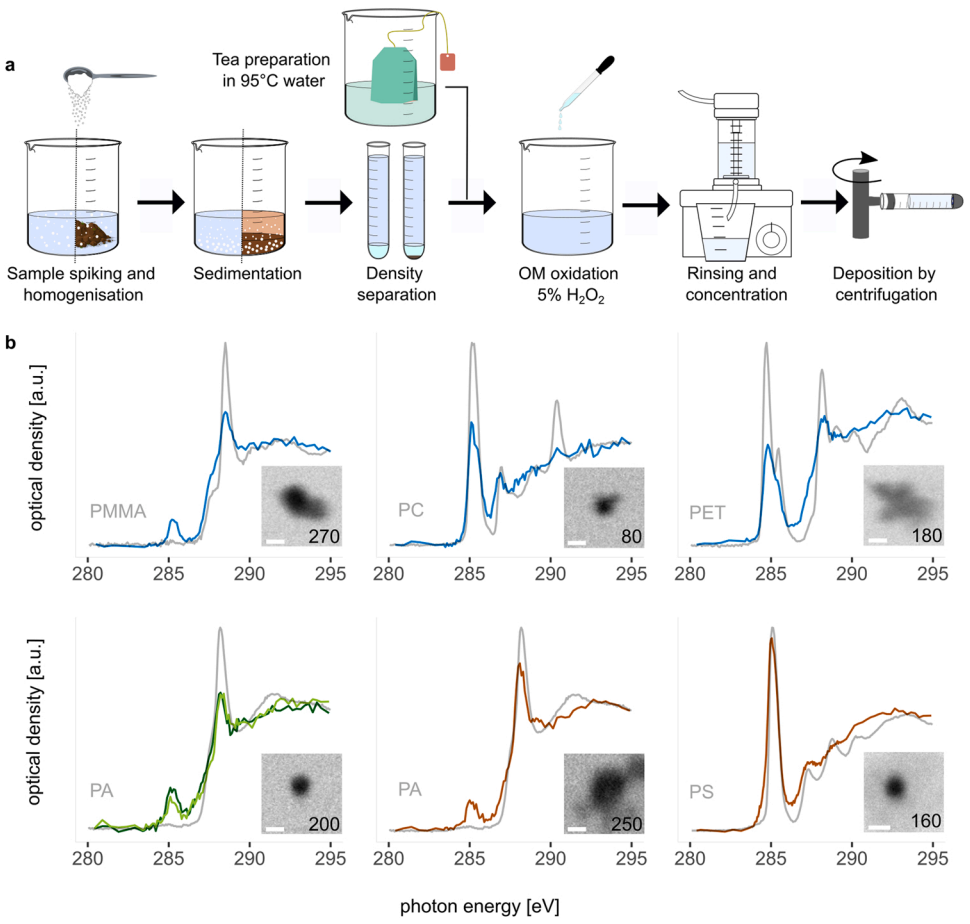

Fig. 3. Identification of NP in spiked water, brewed tea water and spiked soil samples. (a) Schematic representation of the spiking and extraction protocol for water and soil matrices. The water sample was spiked with powder of PMMA, PC, PET and PP. The tea bags were made out of PA. A soil sample was spiked with a powder of PA and another soil sample with 250 nm PS beads. (b) NEXAFS spectra together with a normalized reference spectrum (grey lines, Dhez et al., 2003) and STXM image of the corresponding particle found in the water spiked sample (blue lines), the peppermint and green tea (dark green, light green) and the soils (brown lines). The measured spectra and the corresponding reference were normalized at the pre (280 eV) and post edge (295 eV) energy to fit the scale. The images were acquired at 350 eV and the white scale bar is 250 nm. The number in the image refers to the particle thickness (nm). The small peak at 285 eV, which is not visible in the reference spectra of PMMA and PA but in the spectra from the NP, as well as the differences between the reference and the measure spectra in the 287–293 eV region for PC and PET, are most probably due to radiation damage.

the extraction of metallic nanoparticles (Schwertfeger et al., 2017) and for the purification of MP (Hurley et al., 2018; Liu et al., 2019), with some adaption to NP specific characteristics (e.g., higher sensitivity to oxidation and aggregation) (Schwaferts et al., 2019). With this aim, the density separation was modified to use sucrose to prevent aggregation of NP in concentrated salt solutions like $ZnCl_2$ or NaBr that are often used in MP research (Bläsing and Amelung, 2018; Liu et al., 2019). A gentle oxidation step using low concentration hydrogen peroxide to remove natural organic matter but prevent oxidation of NP and a final ultrafiltration step (Ter Halle et al., 2017) were added to the procedure to clean the samples and preconcentrate the NP prior to their deposition on a silicon nitride membrane by centrifugation. The method was tested on PA NP and was found to have no influence on the NEXAFS spectra of the particles (Fig. S7).

A lake water sample from Lake Lucerne (Switzerland) and a soil sample from a remote mountain soil (Laax, Switzerland) were spiked with NP and then subjected to the above described extraction and analysis procedures. The water sample was spiked with PMMA, PC, PET and PP, and the soil sample, which had proven to be clean from MP and larger plastics (Scheurer and Bigalke, 2018), with PA (Fig. 3, a). In the water sample, NP of PMMA, PC and PET were found (Fig. 3, b blue lines) but not of PP, possibly because too few PP particles spiked were in the NP range (< 1000 nm). In the spiked soil sample, we retrieved the PA NPs (Fig. 3, b, brown line).

3.2.2. *Characterising NP in environmental and food samples*

To assess the suitability of the method to find NP in unspiked food samples, we first analyzed green and peppermint tea prepared from PA teabags (Fig. 3, a). In spite of the high organic matrix of the tea, we were able to differentiate PA from the tea matrix and find PA NP in both tea samples, confirming the previous report of teabags releasing NP in tea infused water (Hernandez et al., 2019) (Fig. 3, b green lines).

For the soils, samples SAN and GAM were collected at agricultural sites where mulching foil had been applied, while samples DUF and BRA were from pasture sites close to roads. In the road site soils we did not check for tire wear particles but for other plastic waste usually found close to roads due to plastic waste thrown out of cars. We found NP of three different polymers (PA, PP, PS) in a size range of 250–900 nm and mostly irregularly shaped (Fig. 4). The presence of PA in the roadside soil can be attributed to NP formation from packaging material waste, while the NP in the arable soils most probably originate from mulch foil, nets and nonwoven covers (PP), strings to fix foil tunnels (PA) and other agricultural applications (PS) (Scarascia-Mugnozza et al., 2011). The fact that no PE (the most commonly used polymer for mulch films) was found, even at the sites with mulching film application, might be either due to PE being a polymer not very susceptible to NP formation (either slow formation or short lifetime) or to the spectrum of aged PE being very similar to natural organic matter and thus, difficult to differentiate.

NP formation has been reported recently in a heavily plastic contaminated soil by AF4 and py-GC-MS (Wahl et al., 2021) and in marine waters (Ter Halle et al., 2017). Our results show the occurrence as well as the characteristics of individual NP in common agricultural soils at common plastic concentrations. The finding of NP in the studied soils show that NP form from larger plastic items in the soils. This NP formation will be favored by physical stress applied to plastic waste occurring in soil such as cutting the grass at roadside soils that will also cut the plastic waste and ploughing at arable soils that might also grind larger plastic items to NP. Beside the physical stress, UV radiation will age plastics as long as they occur at the soil surface and microbial attack might cause disintegration of certain polymers after the plastics are

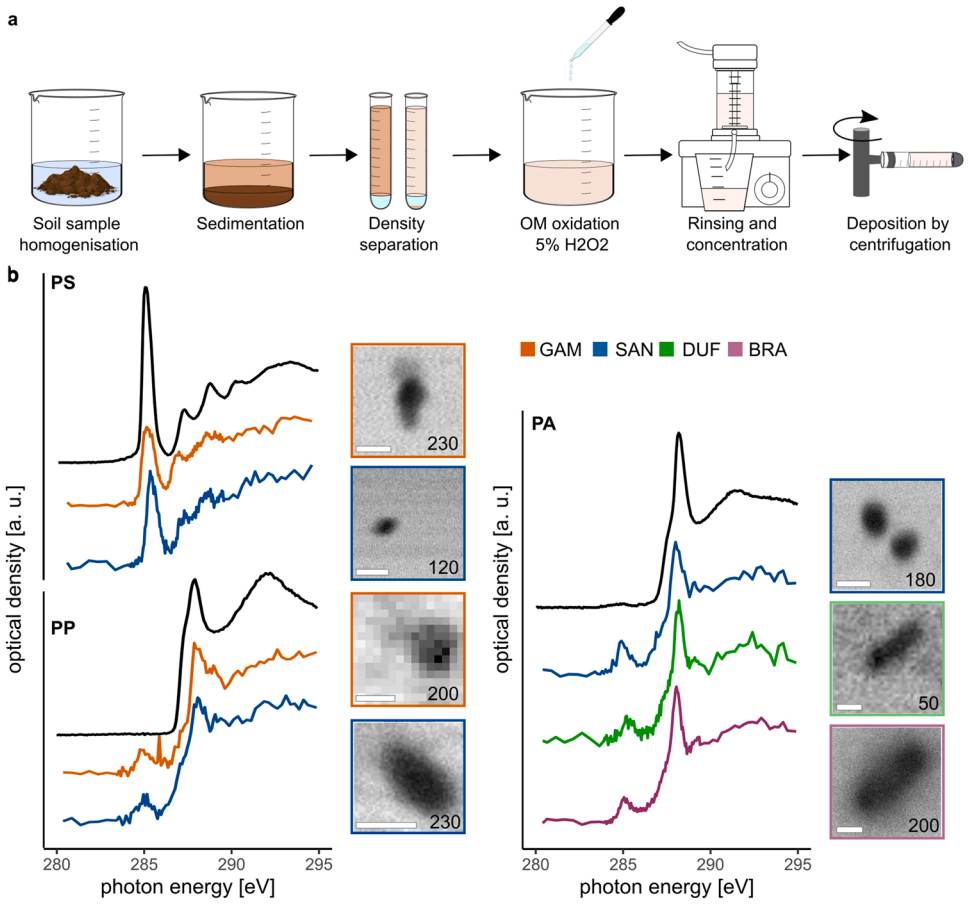

Fig. 4. Identification of NP in 4 natural soil samples. (a) Schematic representation of NP extraction from soil matrices. (b) NEXAFS spectra together with a normalized reference spectrum (grey lines, Dhez et al., 2003) and STXM image of the corresponding particle found in Sant' Antonino (SAN, brown lines), Gampelen (GAM, blue lines), Belpberg Dufti (DUF orange line), and Wohlen b.B Breitacher (BRA, yellow line). The images were acquired at 350 eV. The small peak at 285 eV, which is not visible in the reference spectra of PP and PA but in the spectra from the NP, is most probabaly due to radiation damage. The white scale bar is 500 nm. The number on the image refers to the thickness [nm].

buried into the soil (Otake et al., 1995; Krueger et al., 2015). Beside providing useful insights on NP formation in soils, our results also have implications for the design of ecotoxicological and environmental fate (e.g. transport) studies. While in most such studies, spherical PS/PE NP are used (Thomas et al., 2021) – due to its easy availability and defined shape – our data clearly show that NP from different polymers occur and that their shape is mostly not spherical but rather what is referred as a fragment. Work on engineered nanoparticles has shown that nanoparticle shape has implications for its toxicity (Demir, 2020; Pikula et al., 2020) and transport in porous media (Wang et al., 2016). NP extracted from the marine environment have also been reported to have different toxicities from artificial spherical NP (Baudrimont et al., 2020).

4. Conclusion

We have demonstrated the use of STXM for the imaging and chemical characterisation of individual NP with a minimum dimension down to about 100 nm. We show that it can be applied to the analysis of pure NP and for NP present in environmental and food matrices. While STXM cannot provide statistically significant information on particle numbers, its strength is the high-resolution imaging and spectral investigation of individual particles or complex particle mixtures. For the soil samples analyzed here, three different polymers with different shapes and sizes were found. These results indicate the formation of NP in normal agricultural soils and have implications for future studies on soil nanoparticles and nanoparticle ecotoxicology.

Among the analytical techniques available to analyze the molecular structure of particles, STXM is probably one of the most suitable for the analysis of NP characteristics, because of its high spatial and spectral resolution and the ability to limit radiation damage to the sample. However, STXM analysis of complex samples requires the use of extraction techniques that concentrate NP and eliminate most of the other materials from the sample matrix. Because of the considerable time needed to image particles by raster scanning (1–10 min/image depending on the resolution) and for spectral analysis (10–30 min depending on the dwell time), it is impractical to analyze enough particles to obtain a statistically significant quantification of the NP concentration in a sample. The strength of STXM is instead the differentiation of natural environmental particles (e.g. clay particles, natural organic matter) from NP and to combine imaging with spectroscopy to deliver a full chemical, size and shape characterization of the NP. Due to its high lateral resolution, STXM can trace chemical changes in individual NP or can analyze complex particle aggregates. STXM can be accessed (free of charge for academic use) by any researcher after a successful application to one of the many facilities worldwide (https://lightsources.org; https://wayforlight.eu).

CRediT authorship contribution statement

Alexandra Foetisch: Conceptualisation, Methodology, Software, Validation, Formal analysis, Investigation, Data curation, Writing – original draft, Writing – review & editing, Visualization. **Montserrat Filella**: Conceptualisation, Methodology, Investigation, Writing – review & editing. **Benjamin Watts**: Conceptualisation, Methodology, Software, Investigation, Resources, Data curation, Writing – review & editing, Visualization. **Laure-Hélène Vinot**: Methodology, Validation, Investigation. **Moritz Bigalke**: Conceptualisation, Methodology, Investigation, Resources, Writing – review & editing, Supervision, Project administration, Funding acquisition.

Declaration of Competing Interest

The authors declare that they have no known competing financial interests or personal relationships that could have appeared to influence the work reported in this paper.

Acknowledgments

This study was funded by the Swiss National Science Foundation (SNSF, 200021_182672/1). We acknowledge the Paul Scherrer Institute, Villigen, Switzerland for provision of synchrotron radiation beamtime at beamline PolLux of the SLS and would like to thank Katharina Witte and Simone Finizio for their assistance. We also thank Beatrice Frey from the Department of Chemistry, Biochemistry and Pharmacology of the University of Bern and Agathe Martignier from the Department of Earth Sciences of the University of Geneva, Reto Zanoni from the Veterinary Institute of the University of Bern and Jaime Caplette, Milo Fieber, Daniela Fischer, Adrien Mestrot, Anna Muntwyler, Lucija Stanisic, Gaby Witschi and Evelyn Vonwyl from the Institute of Geography of the University of Bern for helpful suggestions and help in the lab and/or during beamtimes.

Appendix A. Supporting information

Supplementary data associated with this article can be found in the online version at doi:10.1016/j.jhazmat.2021.127804.

References

Abbe, E., 1873. Beiträge zur Theorie des Mikroskops und der mikroskopischen Wahrnehmung. Arch. Für Mikrosk. Anat. 9, 413–468. https://doi.org/10.1007/BF02956173.

Ade, H., Hitchcock, A.P., 2008. NEXAFS microscopy and resonant scattering: Composition and orientation probed in real and reciprocal space. Polymer 49, 643–675. https://doi.org/10.1016/j.polymer.2007.10.030.

Ade, H., Stoll, H., 2009. Near-edge X-ray absorption fine-structure microscopy of organic and magnetic materials. Nat. Mater. 8, 281–290. https://doi.org/10.1038/nmat2399.

Astner, A.F., Hayes, D.G., O'Neill, H., Evans, B.R., Pingali, S.V., Urban, V.S., Young, T.M., 2019. Mechanical formation of micro- and nano-plastic materials for environmental studies in agricultural ecosystems. Sci. Total Environ. 685, 1097–1106. https://doi.org/10.1016/j.scitotenv.2019.06.241.

Baudrimont, M., Arini, A., Guégan, C., Venel, Z., Gigault, J., Pedrono, B., Prunier, J., Maurice, L., Ter Halle, A., Feurtet-Mazel, A., 2020. Ecotoxicity of polyethylene nanoplastics from the North Atlantic oceanic gyre on freshwater and marine organisms (microalgae and filter-feeding bivalves). Environ. Sci. Pollut. Res 27, 3746–3755. https://doi.org/10.1007/s11356-019-04668-3.

Bläsing, M., Amelung, W., 2018. Plastics in soil: analytical methods and possible sources. Sci. Total Environ. 612, 422–435. https://doi.org/10.1016/j.scitotenv.2017.08.086.

Chapman, D.V., Du, H., Lee, W.Y., Wiesner, U.B., 2020. Optical super-resolution microscopy in polymer science. Prog. Polym. Sci. 111, 101312 https://doi.org/10.1016/j.progpolymsci.2020.101312.

Christl, I., Kretzschmar, R., 2007. C-1s NEXAFS spectroscopy reveals chemical fractionation of humic acid by cation-induced coagulation. Environ. Sci. Technol. 41, 1915–1920. https://doi.org/10.1021/es062141s.

Coffey, T., Urquhart, S.G., Ade, H., 2002. Characterization of the effects of soft X-ray irradiation on polymers. J. Electron Spectrosc. Relat. Phenom. 122, 65–78. https://doi.org/10.1016/S0368-2048(01)00342-5.

Demir, E., 2020. An in vivo study of nanorod, nanosphere, and nanowire forms of titanium dioxide using Drosophila melanogaster: toxicity, cellular uptake, oxidative stress, and DNA damage. J. Toxicol. Environ. Health A 83, 456–469. https://doi.org/10.1080/15287394.2020.1777236.

Dhez, O., Ade, H., Urquhart, S.G., 2003. Calibrated NEXAFS spectra of some common polymers. J. Electron Spectrosc. Relat. Phenom. 128, 85–96. https://doi.org/10.1016/S0368-2048(02)00237-2.

Duemichen, E., Eisentraut, P., Celina, M., Braun, U., 2019. Automated thermal extraction-desorption gas chromatography mass spectrometry: A multifunctional tool for comprehensive characterization of polymers and their degradation products. J. Chromatogr. A 1592, 133–142. https://doi.org/10.1016/j.chroma.2019.01.033.

Egerton, R.F., 2009. Electron energy-loss spectroscopy in the TEM. Rep. Prog. Phys. 72, 016502 https://doi.org/10.1088/0034-4885/72/1/016502.

Enders, K., Lenz, R., Stedmon, C.A., Nielsen, T.G., 2015. Abundance, size and polymer composition of marine microplastics ≥ 10 μm in the Atlantic Ocean and their modelled vertical distribution. Mar. Pollut. Bull. 100, 70–81. https://doi.org/10.1016/j.marpolbul.2015.09.027.

Favre, H.A., Powell, W.H., 2014. Nomenclature of organic chemistry: IUPAC recommendations and preferred names 2013. R. Soc. Chem. https://doi.org/10.1039/9781849733069.

Fok, L., Cheung, P.K., Tang, G., Li, W.C., 2017. Size distribution of stranded small plastic debris on the coast of Guangdong, South China. Environ. Pollut. 220, 407–412. https://doi.org/10.1016/j.envpol.2016.09.079.

Geyer, R., Jambeck, J.R., Law, K.L., 2017. Production, use, and fate of all plastics ever made. Sci. Adv. 3, e1700782 https://doi.org/10.1126/sciadv.1700782.

Gillibert, R., Balakrishnan, G., Deshoules, Q., Tardivel, M., Magazzù, A., Donato, M.G., Maragò, O.M., Lamy de La Chapelle, M., Colas, F., Lagarde, F., Gucciardi, P.G., 2019. Raman tweezers for small microplastics and nanoplastics identification in seawater. Environ. Sci. Technol. 53, 9003–9013. https://doi.org/10.1021/acs.est.9b03105.

Glover, P., Mansfield, S.P., 2002. Limits to magnetic resonance microscopy. Rep. Prog. Phys. 65, 1489–1511. https://doi.org/10.1088/0034-4885/65/10/203.

Hashimoto, K., Badarla, V.R., Kawai, A., Ideguchi, T., 2019. Complementary vibrational spectroscopy. Nat. Commun. 10, 4411. https://doi.org/10.1038/s41467-019-12442-9.

Hernandez, L.M., Xu, E.G., Larsson, H.C.E., Tahara, R., Maisuria, V.B., Tufenkji, N., 2019. Plastic teabags release billions of microparticles and nanoparticles into tea. Environ. Sci. Technol. 53, 12300–12310. https://doi.org/10.1021/acs.est.9b02540.

Hitchcock, A.P., Dynes, J.J., Johansson, G., Wang, J., Botton, G., 2008. Comparison of NEXAFS microscopy and TEM-EELS for studies of soft matter. Micron 39, 311–319. https://doi.org/10.1016/j.micron.2007.09.008.

⟨https://lightsources.org⟩.

⟨https://wayforlight.eu⟩.

http://unicorn.mcmaster.ca/aXis2000.html.

Hurley, R.R., Lusher, A.L., Olsen, M., Nizzetto, L., 2018. Validation of a method for extracting microplastics from complex, organic-rich, environmental matrices. Environ. Sci. Technol. 52, 7409–7417. https://doi.org/10.1021/acs.est.8b01517.

Jacobsen, C., 2019. X-ray microscopy. Advances in Microscopy and Microanalysis. Cambridge University Press, Cambridge. https://doi.org/10.1017/9781139924542.

Jiang, B., Kauffman, A.E., Li, L., McFee, W., Cai, B., Weinstein, J., Lead, J.R., Chatterjee, S., Scott, G.I., Xiao, S., 2020. Health impacts of environmental contamination of micro- and nanoplastics: a review. Environ. Health Prev. Med. 25, 29. https://doi.org/10.1186/s12199-020-00870-9.

Krueger, M.C., Harms, H., Schlosser, D., 2015. Prospects for microbiological solutions to environmental pollution with plastics. Appl. Microbiol. Biotechnol. 99, 8857–8874. https://doi.org/10.1007/s00253-015-6879-4.

Leontowich, A.F.G., Hitchcock, A.P., 2012. Secondary electron deposition mechanism of carbon contamination. J. Vac. Sci. Technol. B Nanotechnol. Microelectron. Mater. Process. Meas. Phenom. 30, 030601 https://doi.org/10.1116/1.3698602.

Li, L., Luo, Y., Li, R., Zhou, Q., Peijnenburg, W.J.G.M., Yin, N., Yang, J., Tu, C., Zhang, Y., 2020. Effective uptake of submicrometre plastics by crop plants via a crack-entry mode. Nat. Sustain. https://doi.org/10.1038/s41893-020-0567-9.

Liang, C.-K., Eller, M.J., Verkhoturov, S.V., Schweikert, E.A., 2015. Mass spectrometry of nanoparticles is different. J. Am. Soc. Mass Spectrom. 26, 1259–1265. https://doi.org/10.1007/s13361-015-1151-9.

Liu, M., Song, Y., Lu, S., Qiu, R., Hu, J., Li, X., Bigalke, M., Shi, H., He, D., 2019. A method for extracting soil microplastics through circulation of sodium bromide solutions. Sci. Total Environ. 691, 341–347. https://doi.org/10.1016/j.scitotenv.2019.07.144.

Mamin, H.J., Kim, M., Sherwood, M.H., Rettner, C.T., Ohno, K., Awschalom, D.D., Rugar, D., 2013. Nanoscale Nuclear Magnetic Resonance with a nitrogen-vacancy spin sensor. Science 339, 557–560. https://doi.org/10.1126/science.1231540.

Merkus, H.G., 2009. Particle Size Measurements: Fundamentals, Practice, Quality, Particle Technology Series. Springer, New York?

Mitrano, D.M., Beltzung, A., Frehland, S., Schmiedgruber, M., Cingolani, A., Schmidt, F., 2019. Synthesis of metal-doped nanoplastics and their utility to investigate fate and behaviour in complex environmental systems. Nat. Nanotechnol. 14, 362–368. https://doi.org/10.1038/s41565-018-0360-3.

Nan, C., Yue, W., Tao, L., Yang, X., 2020. Fourier transform infrared nano-spectroscopy: Mechanism and applications. Appl. Spectrosc. Rev. 0, 1–22. https://doi.org/10.1080/05704928.2020.1830789.

Otake, Y., Kobayashi, T., Asabe, H., Murakami, N., Ono, K., 1995. Biodegradation of low-density polyethylene, polystyrene, polyvinyl chloride, and urea formaldehyde resin buried under soil for over 32 years. J. Appl. Polym. Sci. 56, 1789–1796. https://doi.org/10.1002/app.1995.070561309.

Penders, J., Pence, I.J., Horgan, C.C., Bergholt, M.S., Wood, C.S., Najer, A., Kauscher, U., Nagelkerke, A., Stevens, M.M., 2018. Single particle automated Raman trapping analysis. Nat. Commun. 9, 4256. https://doi.org/10.1038/s41467-018-06397-6.

Pikula, K., Chaika, V., Zakharenko, A., Markina, Z., Vedyagin, A., Kuznetsov, V., Gusev, A., Park, S., Golokhvast, K., 2020. Comparison of the level and mechanisms of toxicity of carbon nanotubes, carbon nanofibers, and silicon nanotubes in bioassay with four marine microalgae. Nanomaterials 10, 485. https://doi.org/10.3390/nano10030485.

Popczun, N.J., Breuer, L., Wucher, A., Winograd, N., 2017. On the SIMS ionization probability of organic molecules. J. Am. Soc. Mass Spectrom. 28, 1182–1191. https://doi.org/10.1007/s13361-017-1624-0.

Raabe, J., Tzvetkov, G., Flechsig, U., Böge, M., Jaggi, A., Sarafimov, B., Vernooij, M.G.C., Huthwelker, T., Ade, H., Kilcoyne, D., Tyliszczak, T., Fink, R.H., Quitmann, C., 2008. PolLux: A new facility for soft x-ray spectromicroscopy at the Swiss Light Source. Rev. Sci. Instrum. 79, 113704 https://doi.org/10.1063/1.3021472.

Rodríguez-Hernández, A.G., Muñoz-Tabares, J.A., Aguilar-Guzmán, J.C., Vazquez-Duhalt, R., 2019. A novel and simple method for polyethylene terephthalate (PET) nanoparticle production. Environ. Sci. Nano 6, 2031–2036. https://doi.org/10.1039/C9EN00365G.

Team, R.Studio, 2020. RStudio: Integrated Development for R. Rstudio. PBC, Boston, MA.

Sander, M., Kohler, H.-P.E., McNeill, K., 2019. Assessing the environmental transformation of nanoplastic through 13C-labelled polymers. Nat. Nanotechnol. 14, 301–303. https://doi.org/10.1038/s41565-019-0424-z.

Scarascia-Mugnozza, G., Sica, C., Russo, G., 2011. Plastic materials in European agriculture: Actual use and perspectives. J. Agric. Eng. 14.

Scheurer, M., Bigalke, M., 2018. Microplastics in Swiss floodplain soils. Environ. Sci. Technol. 52, 3591–3598. https://doi.org/10.1021/acs.est.7b06003.

Schwaferts, C., Niessner, R., Elsner, M., Ivleva, N.P., 2019. Methods for the analysis of submicrometer- and nanoplastic particles in the environment. TrAC Trends Anal. Chem. 112, 52–65. https://doi.org/10.1016/j.trac.2018.12.014.

Schwertfeger, D.M., Velicogna, J.R., Jesmer, A.H., Saatcioglu, S., McShane, H., Scroggins, R.P., Princz, J.I., 2017. Extracting metallic nanoparticles from soils for quantitative analysis: Method development using engineered silver nanoparticles and SP-ICP-MS. Anal. Chem. 89, 2505–2513. https://doi.org/10.1021/acs.analchem.6b04668.

Stöhr, J., 1992. NEXAFS Spectroscopy, Springer Series in Surface Sciences. Springer, Berlin Heidelberg, Berlin, Heidelberg. https://doi.org/10.1007/978-3-662-02853-7.

Ter Halle, A., Jeanneau, L., Martignac, M., Jardé, E., Pedrono, B., Brach, L., Gigault, J., 2017. Nanoplastic in the North Atlantic Subtropical Gyre. Environ. Sci. Technol. 51, 13689–13697. https://doi.org/10.1021/acs.est.7b03667.

Thomas, P.J., Perono, G., Tommasi, F., Pagano, G., Oral, R., Burić, P., Kovačić, I., Toscanesi, M., Trifuoggi, M., Lyons, D.M., 2021. Resolving the effects of environmental micro- and nanoplastics exposure in biota: A knowledge gap analysis. Sci. Total Environ. 780, 146534 https://doi.org/10.1016/j.scitotenv.2021.146534.

Wahl, A., Le Juge, C., Davranche, M., El Hadri, H., Grassl, B., Reynaud, S., Gigault, J., 2021. Nanoplastic occurrence in a soil amended with plastic debris. Chemosphere 262, 127784. https://doi.org/10.1016/j.chemosphere.2020.127784.

Wang, J., Morin, C., Li, L., Hitchcock, A.P., Scholl, A., Doran, A., 2009. Radiation damage in soft X-ray microscopy. J. Electron Spectrosc. Relat. Phenom. 170, 25–36. https://doi.org/10.1016/j.elspec.2008.01.002.

Wang, M., Gao, B., Tang, D., 2016. Review of key factors controlling engineered nanoparticle transport in porous media. J. Hazard. Mater. 67.

Watts, B., Ade, H., 2012. NEXAFS imaging of synthetic organic materials. Mater. Today 15, 148–157. https://doi.org/10.1016/S1369-7021(12)70068-8.

Watts, B., Swaraj, S., Nordlund, D., Lüning, J., Ade, H., 2011. Calibrated NEXAFS spectra of common conjugated polymers. J. Chem. Phys. 134, 024702 https://doi.org/10.1063/1.3506636.

Wien, K., 1997. TOF-SIMS analysis of polymers. Nucl. Instrum. Methods Phys. Res. Sect. B Beam Interact. Mater. 131, 38–54. https://doi.org/10.1016/S0168-583X(97)00147-X.

Wöll, D., Flors, C., 2017. Super-resolution fluorescence imaging for materials science. Small Methods 1, 1700191. https://doi.org/10.1002/smtd.201700191.

Zhang, W., Dong, Z., Zhu, L., Hou, Y., Qiu, Y., 2020. Direct observation of the release of nanoplastics from commercially recycled plastics with correlative Raman imaging and scanning electron microscopy. ACS Nano 14, 7920–7926. https://doi.org/10.1021/acsnano.0c02878.